A&A 488, L43–L46 (2008)
DOI: 10.1051/0004-6361:200810246

Astronomy & Astrophysics

Letter to the Editor

Transiting exoplanets from the CoRoT space mission

IV. CoRoT-Exo-4b: a transiting planet in a 9.2 day synchronous orbit⋆,⋆⋆

S. Aigrain[1], A. Collier Cameron[2], M. Ollivier[3], F. Pont[1], L. Jorda[4], J. M. Almenara[5], R. Alonso[4], P. Barge[4], P. Bordé[3], F. Bouchy[6], H. Deeg[5], R. De la Reza[7], M. Deleuil[4], R. Dvorak[8], A. Erikson[9], M. Fridlund[10], P. Gondoin[10], M. Gillon[11], T. Guillot[12], A. Hatzes[13], H. Lammer[14], A. F. Lanza[15], A. Léger[3], A. Llebaria[4], P. Magain[16], T. Mazeh[17], C. Moutou[4], M. Paetzold[18], C. Pinte[1], D. Queloz[11], H. Rauer[9,19], D. Rouan[20], J. Schneider[21], G. Wuchter[13], and S. Zucker[22]

(Affiliations can be found after the references)

Received 22 May 2008 / Accepted 18 July 2008

ABSTRACT

CoRoT, the first space-based transit search, provides ultra-high-precision light curves with continuous time-sampling over periods of up to 5 months. This allows the detection of transiting planets with relatively long periods, and the simultaneous study of the host star's photometric variability. In this Letter, we report the discovery of the transiting giant planet CoRoT-Exo-4b and use the CoRoT light curve to perform a detailed analysis of the transit and determine the stellar rotation period. The CoRoT light curve was pre-processed to remove outliers and correct for orbital residuals and artefacts due to hot pixels on the detector. After removing stellar variability about each transit, the transit light curve was analysed to determine the transit parameters. A discrete autocorrelation function method was used to derive the rotation period of the star from the out-of-transit light curve. We determine the periods of the planetary orbit and star's rotation of 9.20205 ± 0.00037 and 8.87 ± 1.12 days respectively, which is consistent with this being a synchronised system. We also derive the inclination, $i = 90.00^{+0.000}_{-0.085}$ in degrees, the ratio of the orbital distance to the stellar radius, $a/R_s = 17.36^{+0.05}_{-0.25}$, and the planet-to-star radius ratio $R_p/R_s = 0.1047^{+0.0041}_{-0.0022}$. We discuss briefly the coincidence between the orbital period of the planet and the stellar rotation period and its possible implications for the system's migration and star-planet interaction history.

Key words. techniques: photometric – stars: planetary systems – stars: rotation

1. Introduction

Transits provide unique insights into fundamental aspects of extra-solar planets that are currently beyond the reach of other techniques: mean density (via the determination of true masses and radii); atmospheres (using transmission spectroscopy and secondary transit observations); and formation and evolution mechanisms (by means of the statistics of the orbital parameters, including the true mass). All but two of the transiting planets published to date have been very short-period planets (<5 d), whose properties are almost certainly affected by their extreme proximity to their host star. The exceptions are HD 147506b (Bakos et al. 2007) and HD 17156b (Barbieri et al. 2007), with periods of 5.6 d and 21.2 d respectively, which are both in very eccentric orbits ($e \geq 0.5$).

CoRoT is the first space-based transit survey. During its lifetime, it will survey 120 000 stars for up to 5 months with precisions as high as 0.1 mmag per hour. This is the fourth in a series of papers reporting the discovery of new extra-solar planets by CoRoT and associated ground-based follow-up programs. Papers I (Barge et al. 2008) and II (Alonso et al. 2008) presented the discoveries of CoRoT-Exo-1b and CoRoT-Exo-2b, which are both giant planets that are very close to their parent star. Paper III (Bouchy et al. 2008) reported the observation of the spectroscopic transit of CoRoT-Exo-2b. In this paper, we report the detection of CoRoT-Exo-4b, a relatively long period (9.2 d) gas-giant transiting planet. We describe the analysis of its CoRoT light curve, the production of which is described in Sect. 2, to determine both the transit parameters (see Sect. 3) and the stellar rotation period (see Sect. 4). This analysis makes no assumptions apart from the planetary nature of the companion, which was confirmed by ground-based follow-up observations reported in a companion letter (Moutou et al. 2008, hereafter Paper V). In Paper V, the full system parameters are determined using the transit parameters reported in the present work. These parameters are used in Sect. 5, where we discuss the implications of the relatively long period that we measure, and of its close similarity to the stellar rotation period. A further detection, CoRoT-Exo-3b, will be presented in Deleuil et al. (2008, Paper VI).

2. Observations and data processing

As for the other CoRoT planets to date, CoRoT-Exo-4b was first detected during an almost real-time analysis of the raw data, as described in Papers I and II. This detection triggered the ground-based follow-up program described in Paper V, which included ground-based photometry in- and out-of-transit, at higher spatial resolution than the CoRoT observations, to identify which of the stars in the CoRoT aperture was being eclipsed, and multiple radial velocity measurements to derive the companion mass.

⋆ The CoRoT space mission, launched on December 27th 2006, has been developed and is operated by CNES, with the contribution of Austria, Belgium, Brazil, ESA, Germany, and Spain. The first CoRoT data will be available to the public in February 2009 from the CoRoT archive: http://idoc-corot.ias.u-psud.fr/

⋆⋆ Figures 1, 4 and 5 are only available in electronic form at http://www.aanda.org

Table 1. Star and transit parameters derived from the CoRoT light curve. The quantity $M_s^{1/3}/R_s$, which is used in determining the stellar parameters (see Paper V), is derived directly from a/R_S and P.

Parameter	Value	Bayesian range
RA	06 48 46.70	
Dec	–00 40 21.97	
R – mag	13.45	
P_{rot} (d)	8.87 ± 1.12	
P (d)	9.20205 ± 0.00037	
T_0 (HJD)	2454141.36416 ± 0.00089	
i (°)	$90.000^{+0.000}_{-0.085}$	87.708–90.000
a/R_s	$17.36^{+0.05}_{-0.25}$	14.30–17.80
u	$0.44^{+0.16}_{-0.15}$	0.00 – 1.00
R_p/R_s	$0.1047^{+0.0041}_{-0.0022}$	0.1000–0.1125
$M_s^{1/3}/R_s$	$0.899^{+0.003}_{-0.013}$	0.741–0.922

When the planetary nature of the companion was confirmed, a high resolution, high signal-to-noise spectrum of the host star was obtained to derive accurate stellar parameters.

CoRoT-Exo-4 (GSC designation 0480002187), whose coordinates and magnitude are given in Table 1, was observed as part of CoRoT's initial run, during which ~12 000 stars of magnitude $12 < R < 16$ within a $1.3° \times 2.6°$ pointing close to the anticentre of the Galaxy were monitored almost continuously for 58 days, starting on the 6th of February 2007. A total of 72319 flux measurements were obtained for CoRoT-Exo-4. For the first 33 d of the run, the time sampling was 512 s, after which it was switched to 32 s as the transits were detected by the alarm mode.

Aperture photometry was performed onboard using a mask that was automatically selected from a set of 256 templates at the beginning of the run. The same mask was used throughout the run. For stars brighter than $R = 15$, the flux was split along detector column boundaries into broad-band red, green, and blue channels. Although the transits were detected in the raw data, the analysis presented here was based on the pipeline-processed light curve. The pipeline (Auvergne et al. 2008) includes background subtraction and partial jitter correction. For each exposure, a global background level is estimated from a handful of 10×10 pixel background windows distributed over each CCD, excluding background windows affected by hot pixels, and subtracted. The jitter correction is based on the satellite line-of-sight information, which is derived from the asteroseismology channel (which is close to the exoplanet channel on the focal plane). The pipeline only applies a relative jitter correction for the three colour channels. This correction conserves the total (white) flux, and no jitter correction for the total flux is attempted. The pipeline also flags data collected during the SAA or affected by other events likely to impair the data quality, such as entrance into and exit from the Earth's shadow.

The blue channel light curve is affected by a hot pixel event a few days after the start of the observations, which causes a sudden rise in the measured flux followed by a gradual decay of ~5 days. This was corrected by fitting an exponential curve to the decaying segment, excluding a small portion containg a transit (see Fig. 1, online only). This section of the blue channel light curve also shows a gradual rise in flux, which was preserved by adding a linear rise between the local mean flux levels before and after the section of light curve affected by the hot pixel, after subtracting the exponential decay. The red and green channels are free of visible hot pixel events. We note that the transit depth is the same in all three channels (within the uncertainties), as expected for a planetary transit.

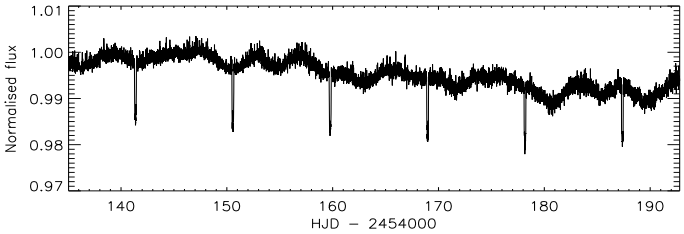

Fig. 2. Pre-processed white light curve of CoRoT-Exo-4. The light curve was normalised by dividing it by its own median, which gives more weight to the later (oversampled) part of the light curve. This does not affect the transit analysis, since it is the local out-of-transit flux around each transit that is taken as a reference (see Sect. 3).

A single band-pass is sufficient for the present work, so the flux from the three colour channels was summed to produce a "white" light curve (covering the range 300–1000 nm). The three-colour photometry will be discussed in an upcoming paper following improvements in the pipeline. A version of the light curve with regular 512 s time sampling was also computed by rebinning there oversampled section of the original. This version was used to study the out-of-transit variability, while the oversampled version was retained to estimate the transit parameters. A short-baseline (5 data points) iterative non-linear filter (Aigrain & Irwin 2004) with 5-σ clipping was applied to both the oversampled and regularly sampled light curves to identify and reject further outliers, resulting in a final duty cycle of 87%.

Based on preliminary ground-based imaging of the field (Deleuil et al. 2006) and an empirical model of the CoRoT PSF, we estimate the contamination of the photometric aperture by stars other than CoRoT-Exo-4 to be 0.3 ± 0.1% (the uncertainty arises from the PSF model). This is compatible with the transit depths measured from the ground (see Paper V). We thus subtracted a constant equal to 0.3% of the median flux, before normalising the light curve (the uncertainty was accounted for separately, see Sect. 3). The full normalised light curve is shown in Fig. 2. We evaluate the actual noise level per 512 s by measuring the dispersion about 1 h (7 exposures) bins, scaling this by $\sqrt{7}$ to give 8.9×10^{-4}, compared to a photon noise level of 5.6×10^{-4}. Possible factors contributing to the difference include residual instrumental effects and the intrinsic variability of the star.

3. Transit analysis

A preliminary ephemeris (orbital period P and epoch T_0) was obtained by computing a least squares fit of periodic, trapezoidal transits to the light curve after filtering out the out-of-transit variations using a 1-day baseline iterative non-linear filter. A more careful removal of the variability was then carried out by fitting a straight line to a light-curve section slightly longer than one transit duration before and after each transit. We experimented with higher order polynomials, but neither improved the dispersion of the residuals, nor changed the results of the subsequent analysis. We folded the corrected segments of light curve using the preliminary period ephemeris, rebinned them into bins of 0.0003 in phase, and fitted the result to obtain preliminary estimates of the system scale a/R_s, the radius ratio R_p/R_s, the inclination i, and the linear limb-darkening coefficient u, where R_s is the star radius, R_p the planet radius and, a the semi-major axis. We varied u instead of fixing its value because reliable theoretical limb-darkening coefficients were not available for the CoRoT bandpass. The ephemeris was then refined by fitting for the time of transit centre T_C for each individual transit event (fixing all other parameters) and fitting a linear relation to the T_C's.

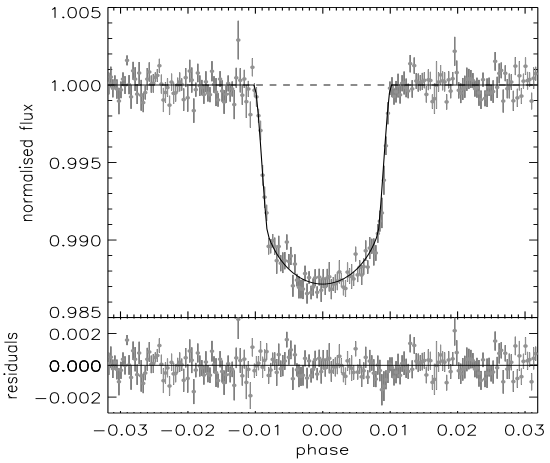

Fig. 3. Folded, binned light curve with the best-fit transit model.

Finally, the light curve was folded again at the refined ephemeris and rebinned to perform a final fit for a/R_s, R_p/R_s, i, and u.

At each stage, we used the formalism of Mandel & Agol (2002) with quadratic limb darkening to generate model transit light curves and the LDL implementation MPFIT of the Levenberg-Marquart fitting algorithm, kindly provided by Markwart, to perform the fit. The period was fixed at the ephemeris value, and the epoch was also fixed except when fitting individual transits. The eccentricity was assumed to be zero (the best-fit solution of the radial velocity data is a circular orbit with an eccentricity uncertainty of 0.1; see Paper V). We also attempted to fit the transits with a quadratic limb-darkening prescription, although this did not improve the fit and we reverted to linear limb-darkening.

To evaluate the noise-induced uncertainties in the transit parameters, including the effect of red noise, we used a 'correlated bootstrap' approach. The residuals from the global best-fit solution were divided into intervals lasting 1.12 h (2/3 of the transit duration, or 1/4 of the duration of the light-curve segments used to calibrate the out-of-transit variations about each transit), randomly shuffled, and added back to the fit before fitting the individual transits. Oversampled and non-oversampled bins were shuffled separately. Each bin was shuffled in its entirety, preserving the detailed time sampling of individual bins; the procedure was not able to describe the effect of small data gaps, but it could account for correlated noise on hour timescales, including the effect of star spots crossed by the planet. We used 100 realisations when fitting individual transits and 1000 when fitting the folded light curve. At each realisation, we also added a constant drawn from a Gaussian distribution with zero mean and standard deviation 0.001 to the data, to account for the uncertainty in the contamination fraction. Since the frequency distributions of each parameter can be significantly non-Gaussian (see in Fig. 4 in the online material), we measure the uncertainties to be the interval between the best-fit value and the point at which the frequency drops below $e^{-1/2}$ times the maximum value (if the distributions were Gaussian, this would be equivalent to the standard deviation). The results are reported in Table 1. For comparison, we also show in Fig. 4 the results of a standard bootstrap, which simply consists of swapping data points, and accounts for white noise only. Apart from the limb-darkening coefficient, the two processes yield similar results, indicating that red noise only slightly affects the other parameters.

To gain an insight into the effect of parameter-to-parameter correlations, we used a Bayesian approach. Reduced χ^2 values were computed over a 4-dimensional grid (i, a/R_s, R_p/R_s, and u) centered on the best-fit solution. A uniform grid in $\cos(i)$ was used, which is equivalent to assuming an isotropic distribution of inclinations. The grid was uniform for all other parameters, i.e. no a priori information for these parameters was assumed, although u was restricted to the physical range 0–1. The χ^2 values were then converted to relative probabilities for each individual model using $p \propto \exp(-\chi^2/2)$ and normalised; probability distributions for each parameter could then be derived shown on Fig. 4) by marginalising over successive parameters. For each parameter, we report in Table 1 the interval over which the probability is higher than the maximum of the distribution multiplied by $e^{-1/2}$. This interval should be interpreted with care: it is not a confidence interval in the frequentist sense, but rather an interval containing ~68% of the posterior probability *integrated over all other parameters*[1]. In the present case, this interval is wide because the global minimum in the multi-dimensional χ^2 surface is narrow, but it is located at one end of a valley that widens significantly away from the minimum, as illustrated in Fig. 4.

In Paper V, the transit parameters are combined with ground-based follow-up observations to infer the stellar and planetary parameters, which we reproduce here for completeness: $T_{\rm eff} = 6190 \pm 60$ K, $\log g = 4.41 \pm 0.05$, $M_s = 1.16^{+0.03}_{-0.02}\,M_\odot$, $R_s = 1.17^{+0.01}_{-0.03}\,R_\odot$, age $1^{+1.0}_{-0.3}$ Gyr; $M_p = 0.72 \pm 0.08\,M_{\rm Jup}$ and $R_p = 1.19^{+006}_{-0.05}\,R_{\rm Jup}$. We note that Claret (2004) computed theoretical linear limb-darkening coefficients in the range 0.55–0.6 for $T_{\rm eff} = 6250$ K and $\log g = 4.5$ in r'; this is the standard bandpass that is closest to the peak of the CoRoT bandpass, although the latter is far broader (300–1000 nm). This range of theoretical limb-darkening coefficients is compatible with the value of 0.44 ± 0.15 obtained from the transit fit.

We checked for transit timing variations in the O–C (observed minus computed) residuals from the refined ephemeris. The results are given in Fig. 5 (online only). The third transit in the time series shows a strong (>500 s) deviation. To test whether this is a real timing variation, we repeated the individual transit fits allowing a/R_s and R_p/R_s to vary as well as T_C; we found a clear correlation between the timing residuals and a/R_s (see bottom left panel of Fig. 5), which points towards the effect of star spots or instrumental systematics rather than a real timing variation as the cause of the outlier. Closer inspection reveals that this transit contains small data gaps, and we interpret the deviation in measured timing and duration as an artefact of these gaps rather than a physical effect. We also checked for a secondary eclipse (removing the variability about phase 0.5 using linear fits as performed for the transits) but none was detected (as expected for this relatively low irradiation planet).

4. Stellar rotation

The light curve in Fig. 2 shows clear out-of-transit variability typical of a rotating, spotted photosphere. Its semi-coherent nature suggests that active regions on the star are evolving on timescales slightly longer than the rotation period. A given active region may therefore cross the visible hemisphere only 2 or 3 times in its lifetime. The shape of the light curve evolves rapidly, but partial coherency should persist for 2 or 3 rotations, implying that autocorrelation is an appropriate method to measure the stellar rotation period. We used an inverse variance weighted adaptation of the Discrete Correlation Function method of Edelson & Krolik (1988) (Collier Cameron et al. 2008) to compute the Auto-Correlation Function, or ACF (see

[1] For an excellent discussion of Bayesian inference and model selection and how it differs from frequentist methods, see Trotta (2008).

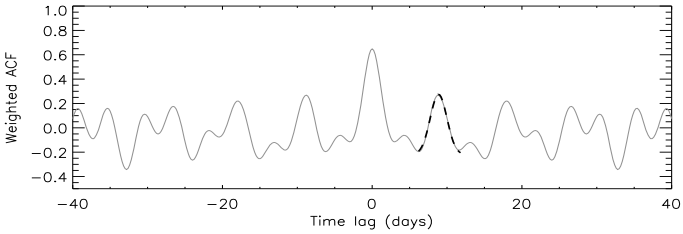

Fig. 6. Weighted autocorrelation function of the out-of-transit light curve (gray line). We estimate the rotation period of the star using a Gaussian fit to the peak of the first side-lobe (dashed black line).

Fig. 6). We fitted a Gaussian to the first peak in the ACF to deduce a period of $P_{\rm ACF} = 8.87 \pm 1.12$ d. The dominant source of uncertainty was the limited duration of the time series. This rotation period is consistent with the $v \sin i$ of 6.4 ± 1.0 km s^{-1} reported in Paper V.

5. Conclusions

The orbital period of CoRoT-Exo-4b is the second longest of any transiting planet to date, following HD 17156b (Barbieri et al. 2007). To our knowledge, it is only the second transiting system for which the stellar rotation period has been measured photometrically (the other being HD 189733, Henry & Winn 2008). There are other systems for which the rotation period and planet orbital period are similar, in particular τ Boo (Catala et al. 2007; Donati et al. 2008) and XO-3 (Johns-Krull et al. 2008; Winn et al. 2008); the rotation periods were derived from Doppler imaging and $v \sin i$ respectively, rather than measured photometrically. In both cases, the stellar rotation period is not identical to the period of the planetary orbit, but is compatible with a synchronised outer envelope when allowing for differential surface rotation. Both planets, which orbit F-type stars similar to CoRoT-Exo-4, are massive and have very short periods (~3 d), and thus may may have induced strong enough tides in the star to synchronise its convective envelope.

Based on the work of Dobbs-Dixon et al. (2004) and Jackson et al. (2008), a simple calculation indicates that CoRoT-Exo-4b, which has a smaller mass and a longer period, would not exert a significant tidal torque on its host star unless tidal energy dissipation occurred at an unphysically high rate in the star. However, McCullough et al. (2008) discussed the case of two other transiting systems containing F-type stars, XO-4 and HAT-P-6, both with orbital periods longer than 7 days, which are roughly half of the (spectroscopically determined) stellar rotation period. They argue that this may indicate the existence of resonant interactions between the planetary orbit and its rotating host star; the absence of these resonances in systems containing cooler stars would then suggest that Jupiter-mass planets can only interact effectively with stars with shallow outer convective zones.

Similarly, if some other factor brought the CoRoT-Exo-4 system to the 1:1 ratio between stellar rotation and orbital period that is observed today, resonant interaction between star and planet may have maintained this ratio thereafter. Any subsequent evolution of the stellar rotation rate is likely to have been modest: 9 d is close to the peak of the rotation period distribution for F-type stars both during the T Tauri phase and in the field (see e.g. Fig. 1 of Barnes 2003). The initial resonance may have occurred naturally if the proto-planetary disk was truncated close to the co-rotation radius, and the planet's migration halted close to the inner edge of the disk. This hypothesis is supported by the absence of detectable eccentricity (see Paper V).

This system clearly warrants further observational and theoretical investigation to constrain its tidal and rotational evolution status further. For example, more detailed analysis of the out-of-transit light curve should enable the active regions on the stellar surface to be mapped in a time-resolved fashion (Lanza et al. 2007) to search for signs of star-planet magnetic interaction.

Acknowledgements. H.D. and J.M.A. acknowledge support from grant ESP2007-65480-C02-02 of the Spanish Science and Innovation ministry, the German CoRoT team (TLS and Univ. Cologne) from DLR grants 50OW0204, 50OW0603, and 50QP0701, AL from contract ASI/INAF I/015/07/0 (work package 3170), and S.Z. from the Israel Science Foundation – Adler Foundation for Space Research (grant No. 119/07).

References

Aigrain, S., & Irwin, M. 2004, MNRAS, 350, 335
Alonso, R., Auvergne, M., Baglin, A., et al. 2008, A&A, 482, L21
Auvergne, M., Bodin, P., Boisnard, L., et al. 2008, A&A, submitted
Bakos, G. Á., Kovács, G., Torres, G., et al. 2007, ApJ, 670, 826
Barbieri, M., Alonso, R., Laughlin, G., et al. 2007, A&A, 476, L13
Barge, P., Baglin, A., Auvergne, M., et al. 2008, A&A, 482, L17
Barnes, S. A. 2003, ApJ, 586, 464
Bouchy, F., Queloz, D., Deleuil, M., et al. 2008, A&A, 482, L25
Catala, C., Donati, J.-F., Shkolnik, E., Bohlender, D., & Alecian, E. 2007, MNRAS, 374, L42
Claret, A. 2004, A&A, 428, 1001
Collier Cameron, A., Davidson, V. A., Skinner, G., et al. 2008, MNRAS, submitted
Deleuil, M., Moutou, C., Deeg, H. J., et al. 2006, in The CoRoT mission: pre-launch status, ed. M. Fridlund, A. Baglin, L. Conroy, & J. Lochard (Noordwijk: ESA), ESA SP-1306, 341
Deleuil, M., Deeg, H., Alonso, R., et al. 2008, A&A, submitted
Dobbs-Dixon, I., Lin, D. N. C., & Mardling, R. A. 2004, ApJ, 610, 464
Donati, J.-F., Moutou, C., Farès, R., et al. 2008, MNRAS, 385, 1179
Edelson, R. A., & Krolik, J. H. 1988, ApJ, 333, 646
Henry, G. W., & Winn, J. N. 2008, AJ, 135, 68
Jackson, B., Greenberg, R., & Barnes, R. 2008, ApJ, 678, 1396
Johns-Krull, C. M., McCullough, P. R., Burke, C. J., et al. 2008, ApJ, 677, 657
Lanza, A. F., Bonomo, A. S., & Rodonò, M. 2007, A&A, 464, 741
Mandel, K., & Agol, E. 2002, ApJ, 580, L171
McCullough, P. R., Burke, C. J., Valenti, J. A., et al. 2008, ApJ, submitted, [arXiv:0805.2921]
Moutou, C., Bruntt, C., Guillot, T., et al. 2008, A&A, 488, L47
Trotta, R. 2008, Contemporary Physics, in press
Winn, J. N., Holman, M. J., Torres, G., et al. 2008, ApJ, submitted, [arXiv:0804.4475]

[1] School of Physics, University of Exeter, Exeter, EX4 4QL, UK
e-mail: suz@astro.ex.ac.uk
[2] Sch. Physics & Astronomy, Univ. St Andrews, St Andrews, KY16 9SS, UK
[3] IAS, Université Paris XI, 91405 Orsay, France
[4] LAM, Université de Provence, 13388 Marseille, France
[5] IAC, E-38205 La Laguna, Spain
[6] IAP, Université Pierre & Marie Curie, 75014 Paris, France
[7] ON/MCT, 20921-030, Rio de Janeiro, Brazil
[8] IfA, University of Vienna, 1180 Vienna, Austria
[9] Institute of Planetary Research, DLR, 12489 Berlin, Germany
[10] RSSD, ESA/ESTEC, 2200 Noordwijk, The Netherlands
[11] Observatoire de Genève, 1290 Sauverny, Switzerland
[12] OCA, CNRS UMR 6202, BP 4229, 06304 Nice Cedex 4, France
[13] Thüringer Landessternwarte, 07778 Tautenburg, Germany
[14] IWF, Austrian Academy of Sciences, 8042 Graz, Austria
[15] INAF - Osservatorio Astrofisico di Catania, 95123 Catania, Italy
[16] IAG, Université de Liège, Liège 1, Belgium
[17] Sch. Physics & Astronomy, Tel Aviv Univ., Tel Aviv 69978, Israel
[18] RIU, Universität zu Köln, 50931 Köln, Germany
[19] ZAA, TU Berlin, 10623 Berlin, Germany
[20] LESIA, Observatoire de Paris, 92195 Meudon, France
[21] LUTH, Observatoire de Paris, 92195 Meudon, France
[22] Dept. Geophysics & Planetary Sciences, Tel Aviv Univ., Tel Aviv 69978, Israel

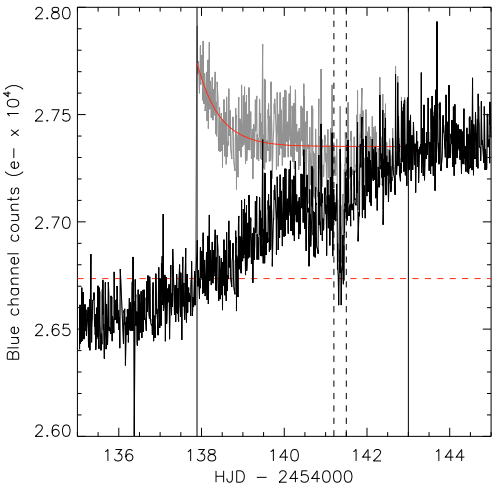

Fig. 1. Correction of the hot pixel event in the blue channel. The light curve before correction is shown in grey, and after correction in black. The vertical solid lines show the time limits of the correction section, with the exponential decay fit shown as a smooth red line. A small subsection, between vertical dashed lines, falls in-transit, and was not used to estimate the correction, although it was corrected. The horizontal dashed line shows the reference flux level adopted before the hot pixel event.

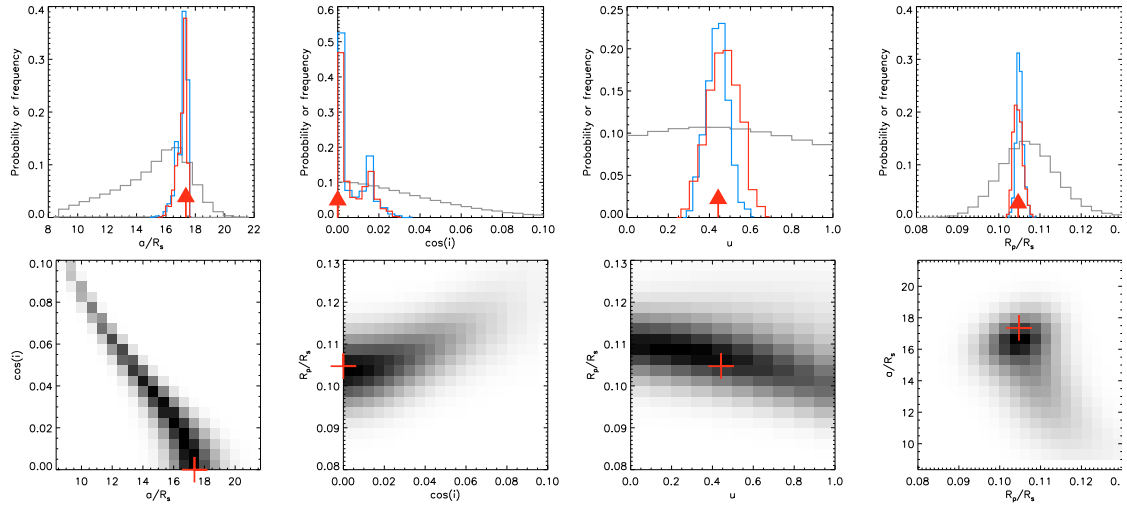

Fig. 4. *Top*: probability and frequency distributions obtained from the Bayesian and bootstrap methods respectively for the main parameters, a/R_s, $\cos(i)$, u and R_p/R_s of the transit fit. The Bayesian method results are shown in grey, the correlated bootstrap in red, and the non-correlated bootstrap in blue. *Bottom*: two-dimensional probability distributions obtained from the Bayesian method for selected pairs of parameters, highlighting the correlations between parameters (particularly a/R_s and i). In each panel, the location of the best-fit model is marked by a red vertical arrow or cross.

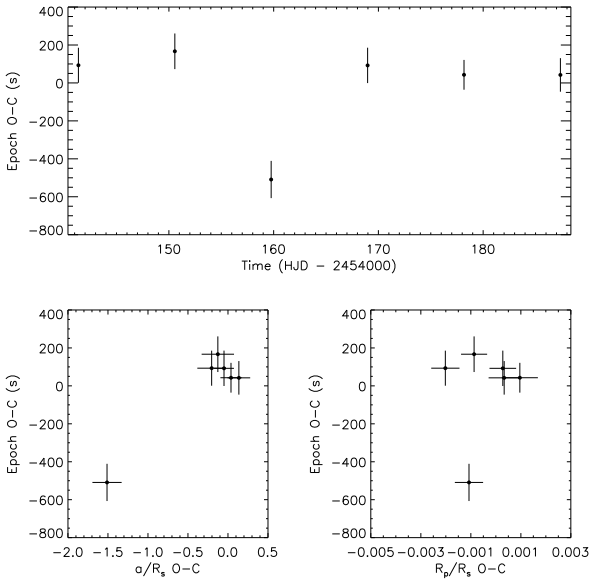

Fig. 5. Transit timing residuals versus time (*top panel*), and versus variations in transit duration (as measured by the scale parameter a/R_s, *left*) and depth (as measured by the radius ratio R_p/R_s, *right*). The apparent timing deviation of the third transit is accompanied by a change in duration, but not in depth. Closer inspection of the light curve shows that this transit is more strongly affected by data gaps than the others.